

Historic microlensing events in the *Euclid* Galactic Bulge Survey

V. Bozza^{1,2}, L. Salmeri¹, P. Rota^{1,2}, E. Bachelet³, J.-P. Beaulieu^{4,5}, A.A. Cole⁴, J.C. Cuillandre⁶, E. Kerins⁷, I. McDonald⁷, P. Mróz⁸, M. Penny⁹, C. Ranc⁵, N. Rektsini⁵, E. Thygesen⁴, H. Verma⁹,
The OGLE collaboration
A. Udalski⁸, R. Poleski⁸, J. Skowron⁸, M. K. Szymański⁸, I. Soszyński⁸, P. Pietrukowicz⁸, S. Kozłowski⁸, K. Ulaczyk¹⁰, K.A. Rybicki⁸, P. Iwanek⁸, M. Wrona^{8,11}, M. Gromadzki⁸, M.J. Mróz⁸,
The MOA collaboration
F. Abe¹², D.P. Bennett^{13,14}, A. Bhattacharya^{13,14}, I.A. Bond¹⁵, R. Hamada¹⁶, Y. Hirao¹⁷, A. Idei¹⁶, S. Ishitani Silva^{13,14}, S. Miyazaki¹⁸, Y. Muraki¹², T. Nagai¹⁶, K. Nunota¹⁶, G. Olmschenk¹³, N.J. Rattenbury¹⁹, Y.K. Satoh¹⁸, T. Sumi¹⁶, D. Suzuki¹⁶, T. Tamaoki¹⁶, S.K. Terry^{13,14}, P.J. Tristram²⁰, A. Vandorou^{13,14}, H. Yama¹⁶

(Affiliations can be found after the references)

Received/ Accepted

ABSTRACT

Context. Microlensing campaigns have a long history of observations covering the Galactic bulge, where thousands of detections have been obtained, including many exoplanetary systems. The *Euclid* Galactic Bulge Survey represents a unique opportunity to revisit a large number of past events and attempt the lens-source resolution of known events falling in the covered area.

Aims. As the analysis of individual events requires non-negligible efforts, it is important to establish priorities among all possible targets, identifying those candidates with the higher chance for a successful resolution of the lens from the source and with the highest scientific interest.

Methods. Drawing from the databases of the three main microlensing surveys (OGLE, MOA and KMTNet), we compile the complete catalog of past microlensing events in the *Euclid* survey footprint up to year 2023, containing 8081 entries. By re-modeling all events and cross-checking with Galactic models, we estimate the relative lens-source proper motions for all events.

Results. Taking into account all uncertainties, for each microlensing event we are able to estimate the probability that the lens is separated from the source by more than a given angular distance threshold. Hence, we rank all events by their resolution probability, providing additional useful information that will guide future analyses on the most promising candidates. A particular attention is dedicated to known planetary microlensing events.

Key words. gravitational lensing: micro; Methods: data analysis; planetary systems

1. Introduction

Gravitational microlensing refers to the temporary increase in the flux of a background source due to the deflection of its light by the gravitational field of an object passing across the line of sight (Paczynski 1986). Following Paczynski's intuition and description of the basic characteristics of the microlensing phenomenon, several astronomers formed collaborations supporting seasonal observational campaigns aimed at the detection of such transient phenomena (Alcock et al. 1993; Udalski et al. 1993). Crowded stellar fields such as the Galactic Bulge offer the highest chance of the alignment needed for microlensing to occur, since stars in the disk or even in the bulge itself may serve as gravitational lenses to background stars (Udalski et al. 1994b; Alcock et al. 2000b; Afonso et al. 2003; Sumi et al. 2003, 2013; Mróz et al. 2019; Nunota et al. 2025). By the photometric measurement of the flux variation throughout the microlensing event, it is generally possible to obtain information about the lens system, regardless of the light from the lens itself, which may even be completely dark. For this reason, microlensing has been first employed to test the possibility

that the dark matter was made of compact objects (Alcock et al. 2000a; Tisserand et al. 2007; Wyrzykowski et al. 2011; Niikura et al. 2019; Mróz et al. 2024b,a), then to study stellar populations in the disk, in the bulge and nearby galaxies, and mostly for the detection of extrasolar planets orbiting the lens stars (Mao & Paczynski 1991; Bond et al. 2004; Gaudi 2012; Tsapras 2018). More recently, a microlensing event has led to the discovery of the first official isolated black hole wandering across our Galaxy (Sahu et al. 2022; Lam et al. 2022).

The duration of a microlensing event is set by the so-called Einstein time t_E , which is the basic observable parameter depending on the mass, distance and relative proper motion of lens and source. Such parameter alone is insufficient to clarify the real nature of an individual lens, since e.g. we may have a massive fast lens or a light slow lens leading to the same Einstein time. Without additional information, microlensing can only be employed in statistical studies on the whole population of lenses. For example, an excess in the number of short events could be due to a population of free-floating planets (Mróz et al. 2017b; Sumi et al. 2023).

Send offprint requests to: V. Bozza, e-mail: valboz@sa.infn.it

There are several ways to break this degeneracy for an individual event: the measurement of the annual parallax is possible for long enough events (Gould 1992), the finite size of the source star intervenes if the impact parameter between the lens trajectory and the line of sight is small enough (Witt & Mao 1994), observations from a satellite may fix the relative parallax between lens and source (Refsdal 1966).

In addition to these methods, we may attempt direct lens detection if we wait long enough to let the lens move away from the glare of the source (Bennett et al. 2006; Beaulieu 2018). It is clear that such detection would immediately return the relative lens-source proper motion. In addition, the lens flux can be used as an additional constraint on the lens mass and distance through the use of stellar models. This technique has been successful in a dozen cases, for which Adaptive Optics (AO) at 10 m-class telescopes has been required or observations from the *Hubble Space Telescope* (*HST*). In several cases, such observations have been able to discriminate between different alternatives and drive microlensing models toward the correct physical description of the event (Bennett et al. 2016; Vandorou et al. 2020; Bennett et al. 2024; Terry et al. 2024b). In all cases, the lens detection has dramatically shrunk the error bars in the mass and distance measurements of the lens (Batista et al. 2014; Bennett et al. 2015; Bhattacharya et al. 2018; Bennett et al. 2020; Blackman et al. 2021; Bhattacharya et al. 2023; Vandorou et al. 2025a).

Indeed, the resolution of the lens from the source is a key element in the strategy devised for the future Galactic Bulge Time Domain Survey (GBTDS) to be performed by the *Roman* space telescope¹ starting from 2027 (Bhattacharya et al. 2019). In fact, by observing the same fields after a few years, *Roman* will likely detect the lenses responsible for most of the microlensing events found in the first season and vice versa. For such events, the uncertainty in the masses of the discovered exoplanets will be significantly reduced, contributing to meeting the science requirements set by the mission goals (Terry et al. 2025).

In the middle between ground-based surveys and the space-based survey by *Roman* comes the ESA *Euclid* mission², which shares many similarities with *Roman* and is an ideal precursor to the NASA mission (Mellier et al. 2025). While engaged with its Wide and Deep surveys, devoted to discover the nature of Dark Energy, *Euclid* has taken a snapshot of the same fields that will be visited by *Roman*. With at least two years span between the *Euclid* images and the first *Roman* observations and a similar Point-Spread-Function (PSF) size, *Euclid* will further increase the chances of lens detections for future microlensing events (Bachelet et al. 2022).

However, the same idea can be implemented looking backward at past microlensing events discovered by ground-based surveys over the past 20 years. For many of the older microlensing events, enough time has passed to see the lens well-separated from the source in *Euclid* images. We thus have an invaluable opportunity to revisit interesting events, such as planetary or binary lenses, validate the past models and reduce the uncertainties of all mass measurements. Besides the published individual events, we have the oppor-

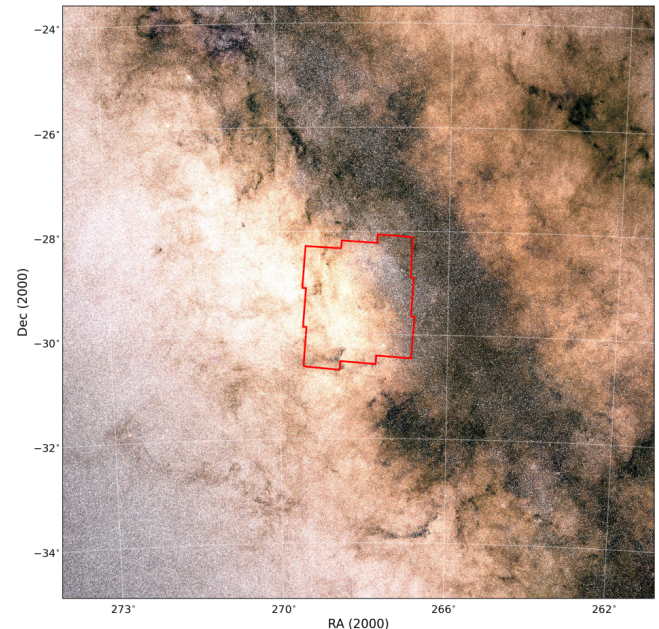


Fig. 1. Outline of the nine Euclid Galactic Bulge Survey pointings (red) overlaid on a Gaia image of the Milky Way. The total outlined sky coverage is 4.8 deg^2 .

tunity to make a much broader statistical study embracing all microlensing events for which we can detect the lens. Population studies can receive a validation by the real flux we see from the lens. Even the non-detection of the lens can be of great value for those short events that may be explained by a fast star or a slow free-floating planet, favoring the second scenario.

For all these reasons, we should not miss the opportunity to use *Euclid* images to boost the overall microlensing collection to a higher level of astrophysical information. As a start-up of this ambitious project, we should first identify all past microlensing events falling in *Euclid* fields and prioritize those that look most promising for the lens detection, trying to re-organize the existing information in such a way that is readily accessible to guide the incoming investigations. This is the goal of the present work. In section 2 we will first describe the *Euclid* Galactic Bulge Survey, we will then describe the sources for past microlensing events in Section 3, presenting some overall statistics on microlensing events in *Euclid* fields. Section 4 will describe the methods we used to assess the probability for lens-source separation for all events. Section 5 brings the focus on published planets involved in this study, for which we have more information available. Finally, we draw the conclusions in Section 6.

2. The *Euclid* Galactic Bulge Survey

The *Euclid* mission was launched on 1st July 2023 and is now orbiting in the Lagrangian point L2, while conducting a survey of the deep sky aimed at an accurate reconstruction of the history of our Universe, clarifying the nature of dark matter and dark energy and the formation of large-scale structures (Mellier et al. 2025). It is made of a Korsch 1.2m telescope with an effective field of view of 0.54 deg^2 (Racca

¹ <https://roman.gsfc.nasa.gov/>

² https://www.esa.int/Science_Exploration/Space_Science/Euclid

Field	RA($^{\circ}$)	Dec($^{\circ}$)
1	267.4250	-30.0194
2	267.4406	-29.2595
3	267.4560	-28.4996
4	268.2266	-30.1299
5	268.2374	-29.3699
6	268.2480	-28.61
7	269.0296	-30.2366
8	269.0355	-29.4766
9	269.0414	-28.7166

Table 1. Reference coordinates of the nine fields of the EGBS.

et al. 2016). In order to keep the telescope and the payload at the temperature of 126K, the telescope is shielded against sunlight and the solar aspect angle must be maintained close to 90° . Further constraints arise to avoid stray light in the optics and affect the survey strategy of the mission. Because of these pointing restrictions, the fields in the Galactic bulge of interest for microlensing can only be viewed in two windows of about 23 days around the equinoxes.

Euclid is able to support the detection and characterization of extrasolar planets by microlensing in two ways: a coordinated time-domain survey of the Galactic Bulge simultaneous with *Roman* to be performed during the allowed pointing windows (Penny et al. 2013; Bachelet & Penny 2019); a single snapshot taken well before the beginning of *Roman* observations (Bachelet et al. 2022). A simultaneous survey would allow immediate parallax determination for most microlensing events observed by the two missions, in particular short events that are amenable candidates for free-floating planets. Such survey could be proposed for an extended *Euclid* mission. A one-time survey of the Galactic Bulge has been performed between 23rd and 24th March 2025 and constitutes the *Euclid* Galactic Bulge Survey (EGBS), to be described here.

Euclid has two wide-field imaging instruments: VIS and NISP, operating in visual and near-infrared bands respectively. NISP was not used in the course of EGBS, so here we briefly describe VIS only. VIS is made of 36 CCDs in a 6×6 array. Each CCD has 4132×4096 pixels in four quadrants, so the VIS images comprise 6.09×10^8 pixels in 144 quadrants (Cropper et al. 2016). The wavelength sensitivity of VIS is $0.53\mu\text{m} < \lambda < 0.92\mu\text{m}$. The plate scale is $0.11''\text{pixel}^{-1}$ which leads to moderate undersampling of the PSF, if we compare with the diffraction limit in the middle of the VIS band, which amounts to about $0.18''$. Since the VIS band is relatively broad, we must also take into account the fact that the PSF is chromatic: redder sources will have a broader PSF. Careful modeling of the PSF is needed to achieve correct photometry and astrometry. For these reasons, the reference observing sequence (ROS) includes 4 consecutive exposures per-field dithered according to a characteristic S-shape pattern. Multiple dithered exposures of the same field allow for a much more accurate reconstruction of the PSF at subpixel level, paving the way to precision astrometry.

The EGBS imaged a total of nine fields in Baade's window. The coordinates of the centers of the fields are reported in Table 1. The fields were rotated by 17° from the north. Fig. 1 shows the fields of the survey superposed on a Gaia image of the Milky Way (Gaia Collaboration et al.

2018). Note that the Galactic center lies on the right, where the extinction becomes more and more severe. We note that some small blank spaces are left between the dithers and the interchip gaps of the VIS instrument.

The exposure time of each dither was 400s. For those stars enjoying more dithers, the limiting magnitude should reach up to AB 25, but this goal will only be verified after the reduction and calibration process of all images will be complete.

Finally, an additional field outside the bulge was pointed with the purpose of facilitating the reconstruction of the PSF at the time of the EGBS.

3. Ground microlensing surveys

Observational campaigns for the detection of microlensing events started back in 1992, with the first project Optical Gravitational Lens Experiment (OGLE) still ongoing (Udalski et al. 1992). After the first pioneering 10 years with only a few events detected per year, the detection of new microlensing events received a boost from automatic alert systems, which were implemented by OGLE, Microlensing Observations in Astrophysics (MOA) and later on by the Korean Microlensing Telescope Network (KMTNet). We will entirely rely on the databases from these three main surveys to compile our list of historic microlensing events.

OGLE observes from the 1.3m Warsaw telescope located in Las Campanas Observatory in Chile. It has undergone several upgrades bringing it to the current phase IV, whose details are described by Udalski et al. (2015). In our catalog we investigate all events detected by OGLE-III and OGLE-IV, ranging from year 2002 to 2023, so as to have a more homogeneous database of events with similar photometric precision, cadence and calibration. Most of these events were alerted in real time thanks to the Early Warning System (EWS) (Udalski et al. 1994a), but we also include some additional events that were recovered offline (Mróz et al. 2019). For the purpose of this paper, we have agreed to use the online photometry available at OGLE online archive³ and use re-reduced photometry only in exceptional cases, as explained in Sect. 4.1. We note that OGLE photometry comes in standard calibrated Cousins I-band, which will represent our standard for our analysis.

MOA observes from the 1.8m MOA-II telescope located at the University of Canterbury's Mount John Observatory in New Zealand (Bond et al. 2001; Sumi et al. 2003). It underwent a major upgrade in 2006, when it started high-cadence observations. We include all events from the MOA archive⁴ starting from year 2000. We also include some anomalous events that were found in offline searches⁵. Similarly to OGLE, we use online photometry for MOA as well. This comes in a customized red band, encompassing standard R- and I-bands. Calibration of MOA data to standard filters requires additional steps that need to be tailored to specific events. In our analysis, therefore, we will incorporate MOA photometry only in the form of instrumental magnitudes.

KMTNet uses three identical 1.6 m telescopes at the Cerro Tololo Inter-American Observatory (CTIO) in Chile,

³ <https://ogle.astrouw.edu.pl/ogle4/ews/ews.html>

⁴ <https://moaprime.massey.ac.nz/moaarchive>

⁵ <http://iral2.ess.sci.osaka-u.ac.jp/~moa/anomaly/bin/index.html>

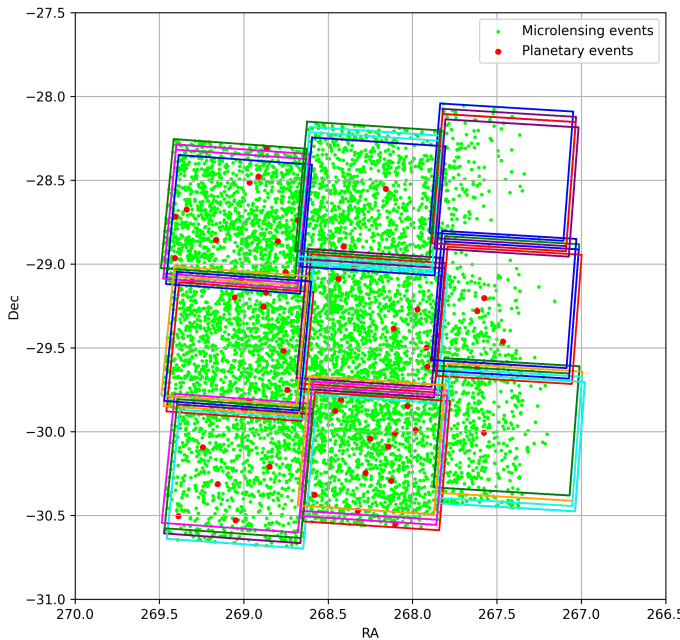


Fig. 2. Fields observed in the EGGS. For each field four different dithers are visible. All historic microlensing events falling in the EGGS are shown in green. In particular, published planetary microlensing events are shown in red.

the South African Astronomical Observatory (SAAO) in South Africa, and the Siding Spring Observatory (SSO) in Australia (Kim et al. 2016) (Kim et al. 2016). As they started observations in 2015, their baseline to EGGS is reduced compared to the other surveys, but still the number of short events found by this survey encourages the use of these data as well. Online public photometry for KMT-Net has been used⁶. We have used their I-band photometry which has a sufficiently good calibration for our purposes.

4. Historic microlensing events in EGGS

The EGGS frames come with WCS astrometry for a precise reconstruction of the field coordinates. This allows us to easily check the presence of each of the past microlensing events discovered from the ground in the footprint of the EGGS. In the public repository <https://github.com/euclid-eggs/HistoricList> we have provided a script that returns the file names and the corresponding pixel coordinates in which an event in given astronomical coordinates appears.

Using this tool, we have selected the historic events imaged by *Euclid* among all ground surveys, collecting 8081 independent events. They are shown in Fig. 2 along with the EGGS fields. The decrease of events on the western side due to the increase of dust extinction as we approach the Galactic center is clearly visible. Within these events, we find 51 published planetary events, highlighted in red in the figure. These obviously constitute the targets of highest interest for the exoplanet community and will receive priority for the identification of the lenses. Among the most interesting events, we may mention OGLE-2006-BLG-109, the first multiplanetary event (Gaudi et al. 2008; Bennett et al. 2010), MOA-2011-BLG-293, for which the

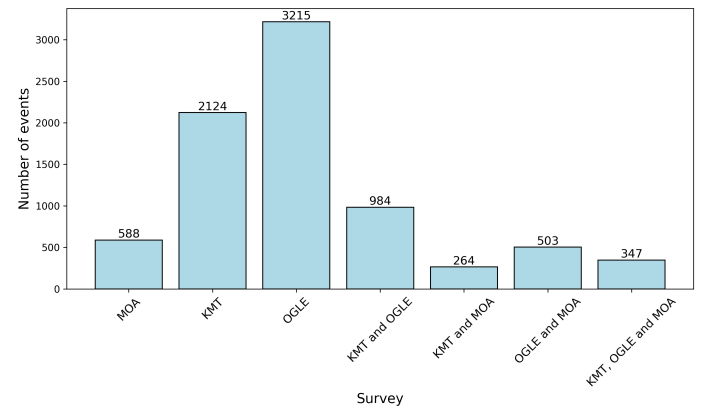


Fig. 3. Distribution of events per survey. Some events have been observed by more than one survey.

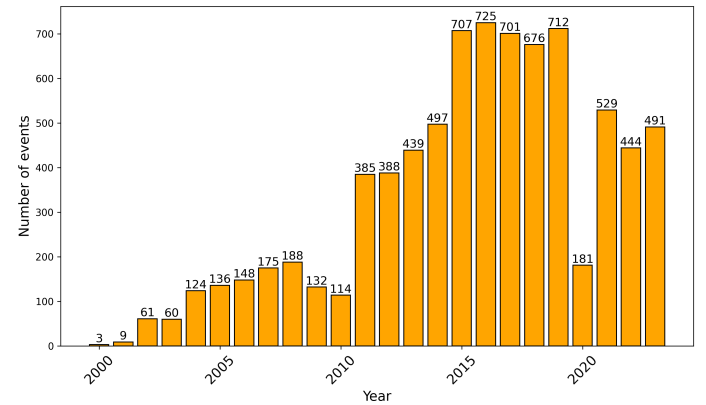


Fig. 4. Distribution of events per year.

lens has already been detected by Keck and is a candidate planet in the habitable zone (Batista et al. 2014), OGLE-2005-BLG-390, a system with an icy 5.5 Earth-masses planet (Beaulieu et al. 2006), the Earth-mass planet OGLE-2016-BLG-1195b (Bond et al. 2017; Shvartzvald et al. 2017; Vandorou et al. 2025b), OGLE-2017-BLG-0173, a planet in a “Hollywood” event Hwang et al. (2018b), the multiplanetary system OGLE-2018-BLG-1011 (Han et al. 2019), OGLE-2013-BLG-0341, a planet in a binary system (Gould et al. 2014), OGLE-2015-BLG-0966, OGLE-2018-BLG-0596 and OGLE-2017-BLG-0406, also observed by *Spitzer* (Street et al. 2016; Jung et al. 2019; Hirao et al. 2020), OGLE-2011-BLG-0462, the first isolated black hole discovered by microlensing (Sahu et al. 2022; Lam et al. 2022), the free-floating planet candidates KMT-2019-BLG-2073 (Kim et al. 2021) and OGLE-2017-BLG-0560 (Mróz et al. 2019).

Fig. 3 contains an overview of the events in EGGS divided by surveys. Some of the events have been observed by more than one survey. In this case, all the data are included in the re-analysis of Sect. 4.1. Fig. 4 shows the distribution of events per year of discovery. We note that a first boost in the number of events came in 2011 with the onset of OGLE-IV and another boost in 2015 is due to the start of the KMTNet project. The interruption in 2020 due to the Covid pandemic is also evident.

For each of these events, the surveys provide synthetic information on their web pages. This includes co-

⁶ <https://kmtnet.kasi.re.kr/ulens/>

ordinates, a finder chart, some parameters obtained by single-lens-single-source fitting: the baseline magnitude, the peak epoch, the Einstein time, the peak magnification or the impact parameter. Finally, some comments are sometimes posted about interesting or problematic events. For all events, online photometry is also available, which is the basis for our re-modeling.

4.1. Re-modeling of events

Our goal is to compile a ranking of all microlensing events in EGGS based on the probability that the lens can be resolved by *Euclid* observations. Therefore, we need a full homogeneous re-analysis of all microlensing events with the same modeling platform and with the same criteria, also including binary lens and/or binary source modeling. The main parameters we wish to extract are the Einstein time and, when measurable, the microlensing parallax, due to the orbital motion of the Earth.

The Einstein time is the ratio between the Einstein angle θ_E and the relative lens-source proper motion μ_{geo} as seen from the Earth at the time of the microlensing event:

$$t_E \equiv \frac{\theta_E}{\mu_{geo}}. \quad (1)$$

The Einstein angle fixes the lensing power of the event and is given by:

$$\theta_E \equiv \sqrt{\kappa M \pi_{rel}}, \quad (2)$$

where M is the mass of the lens, $\pi_{rel} = \pi_L - \pi_S$ is the difference of the geometric parallaxes of lens and source, and $\kappa = 4G/c^2$ au combines the Newton constant, the speed of light and the astronomical unit.

The microlensing parallax

$$\pi_E \equiv \frac{\pi_{rel}}{\theta_E} \quad (3)$$

can be measured for long enough events for which the Earth orbital motion is relevant or by satellite observations.

Finally, the source physical size can affect the microlensing light curve sometimes. The parameter

$$\rho_* \equiv \frac{\theta_*}{\theta_E} \quad (4)$$

can be useful if the angular size of the source θ_* can be estimated by stellar models.

In general, in order to fully break the degeneracy between the proper motion μ_{geo} , the lens mass M and the distances to lens $D_L \equiv \text{au}/\pi_L$ and source $D_S \equiv \text{au}/\pi_S$, it is necessary to have a good measurement of π_E and ρ_* , coupled with some hypothesis on the source through stellar models. It is clear that this is not possible for the vast majority of the microlensing events under examination in this investigation because finite-size effects are very rare, the microlensing parallax is less rare but not typically measured, in particular for short time-scale events, which are the most promising to be resolved by *Euclid*. Finally, a color-magnitude diagram (CMD) could be used to investigate the nature of the microlensing source, so as to estimate θ_* or to infer the source distance, but not all events have available color information in the target field.

Therefore, we will just compile our ranking based on the simplest information we can extract from our models: t_E and π_E when possible, and obviously the baseline magnitude I_{base} and the peak epoch t_0 . The use of ρ_* would require a CMD investigation for each event, which is clearly out of reach. The situation is different for published planetary events, for which the full investigation is already publicly available. We will dedicate a separate section (Section 5) to these events.

Having re-framed the scope of our re-modeling to I_{base} , t_E and π_E , it is clear that the online photometry is generally sufficiently good to achieve such limited goal. In fact, the purpose of re-reduction by sophisticated pipelines is to improve the accuracy so as to reveal subtle features or anomalies in the light curve. While such work is of primary importance to detect and characterize planets correctly, it has very little impact on global parameters such as the time-scale of the event, which sets the Einstein time. The microlensing parallax may be affected by long-term systematics that could be present in online photometry, but given the lower priority of long time-scale events in our list, we accept the possibility that our estimate of parallax may be altered by systematics in some of these events. There is certainly no sufficient motivation to enterprise a titanic work of re-reduction of 8081 events only to adjust a few probabilities that remain very low anyway.

The modeling platform chosen for the re-analysis of all microlensing events in EGGS is **RTModel**⁷ (Bozza 2024), which provides models in the single-lens-single-source, binary-source and binary-lens categories and proposes an assessment based on a comparison of the χ^2 achieved by each model category. The initial conditions for fitting are taken from a grid search for single-lens models and from a template library for binary-lens models. The fitting algorithm is a Levenberg-Marquardt with a bumping mechanism preventing duplicates and enlarge the exploration of the parameter space. The code employed for the computation of microlensing magnification is **VBMicrolensing** (Bozza et al. 2025).

To speed-up the analysis for each event, we only include the data collected in the year of the peak, except for those events whose peak falls in-between two seasons. The remaining data are re-binned down to a maximum of 1000 data points. Such re-binning, as performed by **RTModel** preserves light curve variations and only acts on constant sections of the light curve (typically along the baseline), so it has virtually no impact on the inferred t_E .

For each event, we record the following information, useful for the estimate of the lens-source proper motion and the resolution probability:

- best model category in the letter coding used by **RTModel**;
- $\chi^2/d.o.f.$;
- Einstein time t_E ;
- baseline magnitude I_{base} ;
- microlensing parallax π_E ;

The $\chi^2/d.o.f.$ can be considered as an assessment of the reliability of the model. A high value can be determined by the presence of intrinsic scatter in the data, outliers, by an inaccurate model or by the presence of a non-microlensing

⁷ <https://github.com/valboz/RTModel>

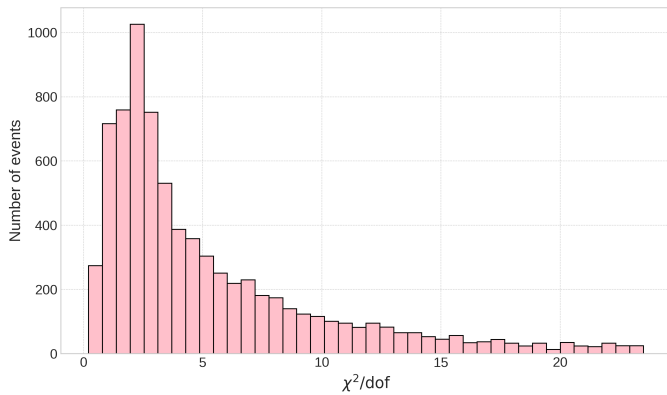


Fig. 5. Distribution of events in terms of the $\chi^2/d.o.f.$ achieved in their fit.

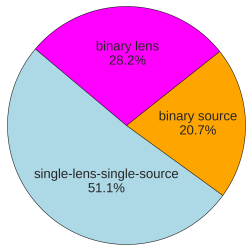


Fig. 6. Incidence of different model categories as found by RTModel1. As explained in the text, we caution the reader that the abundance of binary lens/source events found in this analysis is a natural consequence of the presence of occasional outliers in the online photometry, which has been adopted in this study and does not reflect the real distribution of microlensing events.

signal (periodic or eruptive variables). Fig. 5 shows the distribution of this indicator on the modeled events. The mode is in the bin $1.5 < \chi^2/d.o.f. < 2$, which seems reasonable in consideration of the fact that even a few outliers or low-level systematics may lift the value from unity. The very long tail towards high values is dominated by KMTNet events for which the online photometry is very poor. This does not automatically mean that the fit found by RTModel1 is wrong. In most cases, RTModel1 catches the essentials of the microlensing event in spite of the high scatter. However, this diagnostics will warn the user that the data or the model for the event may present some problems or peculiarities that require further investigation.

The numbers of events falling in the three main categories (single-lens-single-source, binary-source, binary-lens) are reported in Fig. 6. As expected, the majority of events is made by single-lens-single-source, but nearly half of the events is classified as binary-lens or binary-source. Besides genuine binaries, it is certainly possible that scatter in the baseline can sometimes mimic an anomaly that is reported as a signature of a binary-lens or a binary-source. This is a consequence of the adoption of online photometry, which is naturally plagued by outliers or noise that would be removed by targeted photometry. RTModel1 obviously finds a decrease in χ^2 by adding lenses and sources on problematic points of these light curves. However, such short-term false anomalies do not spoil the measurement of the Einstein time, which is fixed by the longer-scale genuine microlensing signal. In principle, we may lower our threshold

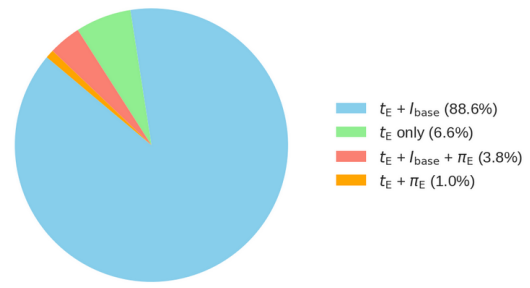


Fig. 7. Events classified according to measured observables.

for rejection of outliers, but this would put real short time-scale events in danger. So, between the two alternatives, we choose to have correct Einstein times on misclassified events rather than wrong Einstein times on short events.

We were not able to extract I_{base} and π_E for all microlensing events. As already anticipated, for MOA-only events we are unable to have a good enough calibration to estimate I_{base} . The microlensing parallax is measurable only for a minority of events. Fig. 7 quantifies the numbers of events based on the measured parameters. Almost 90% of events are assessed based on the measured t_E and baseline magnitude I_{base} . Parallax is measured in 1% of events.

Fig. 8 shows the distribution of events in terms of the baseline magnitude I_{base} . This reflects the luminosity function in the bulge, with a decline for $I > 20$ following the difficulty of performing accurate photometry from the ground for such faint sources.

Fig. 9 contains the distribution of the events in the Einstein time t_E , whose Gaussian shape peaking at 20 days closely resembles similar distributions obtained by the surveys (Sumi et al. 2023; Mróz et al. 2017b). Only the events with an uncertainty on t_E lower than t_E itself are displayed. Einstein times longer than one year are unreliable because we have used one or two seasons at most. As stated before, we are not interested in such long events as they have negligible chance of being resolved at the time of EGGS. For this reason, Fig. 9 is truncated at $t_E < 1$ year. On the other side, we note that there are some very short events, which are associated with faster lens-source relative proper motion leading to higher chances for the resolution in *Euclid*. These events may be also due to free-floating planets and thus deserve to be treated with the highest care. We have therefore inspected by eye all these short events to check that they are genuine microlensing events.

4.2. Galactic model and estimated proper motion

After the re-modeling described in the previous sub-section, for each microlensing event in EGGS we now have robust estimates of the basic parameters, such as Einstein time, baseline magnitude and microlensing parallax. As said before, this is not sufficient to fully break the degeneracy between mass, distance and proper motion. In order to make a prediction on the probability of separating the lens from the source, we must rely on prior expectations from our knowledge of the Galactic stellar populations. Their space distribution and their kinematics provide guidance on the most likely ranges for the proper motion of each microlensing event. Crossing this prior expectation with the constraints

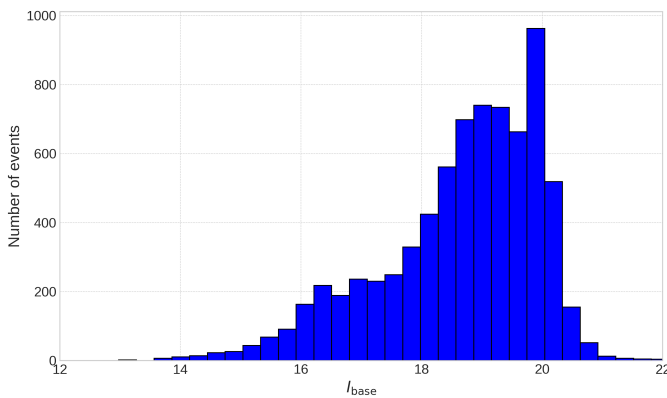


Fig. 8. Distribution of events in terms of the baseline magnitude in I-band.

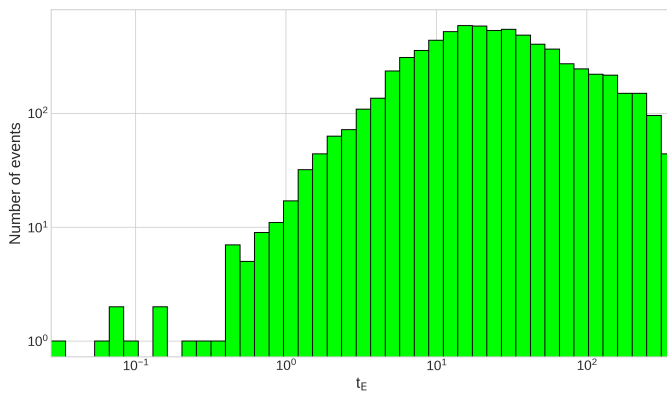


Fig. 9. Distribution of events in the Einstein time t_E .

coming from our measured parameters, we can derive posterior probability distributions for the proper motion that can be used to infer the expected lens-source separation for each microlensing event.

There are several Galactic models designed for such a Bayesian approach in microlensing analysis (see e.g. Robin et al. (2003); Han & Gould (2003); Dominik (2006); Yang et al. (2021)). A massive data analysis like the one we have to do for 8081 microlensing events requires a fast, easy and reliable code that can be easily scripted. We have adopted the software `genulens`⁸ (Koshimoto & Ranc 2022), based on the model by Koshimoto et al. (2021), which incorporates stellar density and kinematic information from *Gaia* (Gaia Collaboration et al. 2018), OGLE (Nataf et al. 2013; Mróz et al. 2019) and radial velocity surveys (Clarke et al. 2019; Kunder et al. 2012) for a better characterization of the bulge.

For each microlensing event, we provide `genulens` with all available information that affects the proper motion distribution. Firstly, the Galactic coordinates determine the line of sight and the stellar populations potentially contributing as sources or lenses. The Einstein time t_E and the microlensing parallax π_E , when available provide basic constraints on the velocities, mass and distance of the lens through Eqs. (1-3). The baseline magnitude I_{base} places an upper limit to the mass for both the source and the lens (if it is a star). In order to exploit this information, we must

also estimate the extinction in the I-band. Since we cannot construct a CMD for all microlensing events, we rely on existing extinction maps. In particular, we have chosen the fast and scriptable platform from NASA/IPAC infrared science archive⁹, based on COBE/DIRBE and IRAS/ISSA surveys (Schlegel et al. 1998), updated with Sloan Digital Sky Survey (Schlafly & Finkbeiner 2011). Although these maps may not capture small-scale variations in the extinction, they should be accurate enough for the purpose of applying the baseline constraint to our microlensing events.

In the end, for each microlensing event, we get the distribution of the heliocentric proper motions compatible with the characteristics of our event. A few representative examples are shown in Fig. 10.

4.3. Lens detection probabilities in historic events

The posterior distribution for the heliocentric proper motion can be immediately translated to a distribution in the expected lens-source separation after multiplying the proper motion by the time baseline between the microlensing peak epoch t_0 and the EGGS time $HJD \simeq 2460758 \pm 1$. At this point, we are in the position to estimate the probability that the lens-source separation exceeds our desired threshold.

Table 2 contains an excerpt of 20 events from the full list of 8081 historic microlensing events available at <https://github.com/euclid-eggs/HistoricList>. For each event we report the modeling parameters together with the probabilities that the lens-source separation exceeds four reference thresholds: 0.18", corresponding to the average FWHM of the PSF for the VIS instrument; 0.11", the pixel angular scale in VIS; 0.055", half-pixel scale; and 0.0275", a quarter pixel scale. The real threshold for a successful detection of the lens as a separate object from the source depends on the relative flux ratio, the total flux, the color difference between source and lens, the crowding, the presence of the target on multiple dithers. For this reason, we have provided different thresholds that may apply to different cases.

Some interesting overall statistics can be drawn from this table. Fig. 11 shows the number of events with detection probability higher than the value in the abscissa assuming one of the four reference threshold. All curves start from 8081, since all events have a probability higher than 0%, and terminate to zero at 100%. For example, we can see that the number of events with probability higher than 50% of having lens and source separated by more than 0.0275" is 5595. In other words, we expect 69% of all microlensing events to be separated by more than 1/4 pixel. Similarly, 38% of all events have a higher than 50% probability of being separated by more than 0.055", and still 4.2% of events should be separated by more than 0.11", corresponding to one full pixel. Such values remind us that a generic historic microlensing event will still have lens and source unresolved in *Euclid*. This also enforces the need of identifying the most promising microlensing events which should be considered in the first place in our analysis. Table 2 is sorted by decreasing resolution probability, with the most promising candidates on top of the list. Indeed, the top lines are dominated by short events that have been observed more than 20 years ago. Again we have checked by

⁸ <https://github.com/nkoshimoto/genulens>

⁹ <https://irsa.ipac.caltech.edu/applications/DUST/>

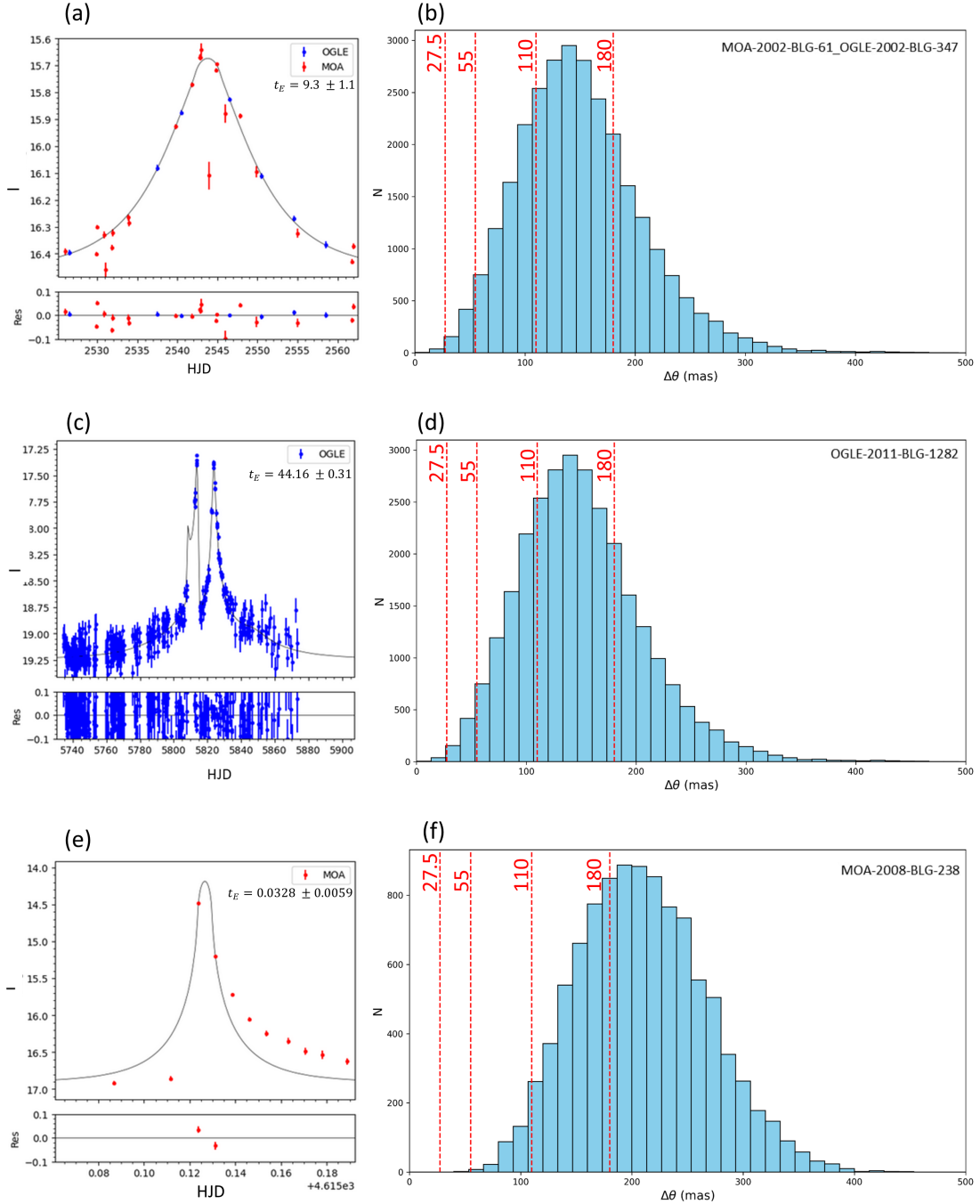


Fig. 10. Three representative historic events. (a) Light curve for the single-lens-single-source event MOA-2002-BLG-61/OGLE-2002-BLG-347 and (b) the probability distribution for the lens-source separation for this event as calculated by `genulens` using the Einstein time obtained by `RTModel`. We have also marked the four thresholds used in the compilation of Table 2. (c)-(d) refer to the binary lens OGLE-2011-BLG-1282. (e)-(f) MOA-2008-BLG-238 is an example of a non-microlensing event in the historic sample, probably triggered by an eruptive variable.

eye inspection the top 100 events, removing some false positives, such as dubious microlensing events or clear eruptive variables.

Fig. 12 shows the distribution of the events with probability higher than 50% for each reference threshold per year of detection. We see that higher thresholds are only accessible to older events, while lower thresholds still allow some more recent events to pass the selection.

5. Known microlensing planets

The list of historic microlensing events also contains 51 published planetary events, which surely attract the greatest attention. In fact, the perspective of resolving the lens from the source for such events allows for a much more accurate mass estimate for the planet and the properties of the planetary system, including a more detailed view on the host star.

Known planetary events have already been investigated in detail and the results are publicly available in the re-

Table 2. An excerpt of the list of historic microlensing events in EGGBS footprint. The full table is available at <https://github.com/euclid-egbs/HistoricList>. For each event we report the probabilities (percentages) that the lens-source separation exceeds the indicated threshold in mas. We also report the model inferred by **RTModel** (single-lens-single-source (PS), binary lens (LS), binary source (BS)), the Einstein time t_E in days, the baseline magnitude, if available, the peak time t_0 in $HJD - 2450000$, the extinction A_I and the χ^2/dof .

Event	P(>180)	P(>110)	P(>55)	P(>27.5)	Model	t_E	I_{baseline}	t_0	A_I	χ^2/dof
MB000003	46.344	85.738	98.798	99.928	PS	6.060 ± 1.747	N.A.	1692.160	1.999	1.069
MB000007	45.503	85.548	98.680	99.910	PS	5.960 ± 0.993	N.A.	1725.789	1.423	0.769
OB020198	39.542	83.327	98.662	99.920	PS	4.970 ± 1.644	17.524	2445.986	1.628	2.627
OB020139	38.661	81.209	98.502	99.947	BS	4.115 ± 10.949	16.643	2436.010	2.228	1.395
OB040538	35.274	80.195	98.073	99.897	PS	3.230 ± 0.599	18.231	3252.214	1.318	2.856
MB040035	34.975	79.841	98.234	99.918	LS	3.532 ± 0.103	N.A.	3185.605	1.826	4.281
OB060146	33.969	79.451	98.462	99.928	PS	1.056 ± 1.029	17.374	3837.844	1.732	1.753
OB050373	33.943	79.230	98.025	99.916	PS	3.054 ± 0.496	17.856	3559.319	2.028	2.425
MB040001-OB040065	33.382	79.604	98.162	99.900	PS	4.435 ± 0.298	16.712	3070.501	1.958	1.629
OB040061	32.942	80.113	98.252	99.887	PS	4.887 ± 1.973	17.473	3070.038	1.406	1.301
OB040162	32.047	79.049	97.990	99.869	PS	4.632 ± 0.466	18.463	3111.095	1.503	5.971
OB040060	31.574	78.734	98.074	99.844	BS	4.776 ± 0.504	15.858	3069.638	1.439	4.503
OB020329	31.524	76.666	97.924	99.877	PS	10.378 ± 6.194	16.522	2522.621	1.694	3.027
OB040002	31.288	78.700	98.013	99.860	PS	4.537 ± 0.842	16.960	3051.573	1.537	1.336
OB030425	31.248	78.583	98.141	99.862	PS	6.102 ± 2.101	16.928	2902.429	1.372	3.204
OB040115	30.809	78.414	98.090	99.871	PS	5.574 ± 1.922	17.380	3094.553	1.875	1.946
OB030326	30.563	78.522	97.954	99.901	LS	5.572 ± 0.560	15.569	2863.711	2.197	1.498
OB030120	30.392	72.098	96.499	99.801	PS	8.578 ± 28.214	16.344	2755.187	2.088	1.282
OB060344	29.584	77.979	98.048	99.890	PS	2.631 ± 1.465	19.846	3905.224	1.743	1.085
OB040064	29.573	78.189	97.774	99.848	PS	6.004 ± 0.553	17.424	3073.035	3.137	1.543
OB020372	29.489	72.797	97.129	99.858	PS	13.956 ± 15.628	16.347	2565.058	1.907	1.124

Table 3. An excerpt of the table of planetary events falling in EGGBS footprint. The full table is available online at <https://github.com/euclid-egbs/HistoricList>. For each event we report the expected lens-source separation; if more than one model exists, we report all possibilities. The method used in the reference paper to constrain the proper motion can be Finite-Source (FS), parallax (PX), High-Resolution imaging (HR), or a combination of these methods.

Event	$\delta\theta$ (arcseconds)	Method	Reference
OB050390	0.142 ± 0.035	FS	Beaulieu et al. (2006)
MB130260-OB130341_M1	0.127 ± 0.010	PX	Gould et al. (2014)
KB160212_M2	0.119 ± 0.039	FS	Hwang et al. (2018a)
KB160212_M3	0.098 ± 0.030	FS	
KB160212_M4	0.088 ± 0.030	FS	
KB160212_M1	0.073 ± 0.023	FS	
OB151771_M3	0.100 ± 0.014	FS	Zhang et al. (2020)
OB151771_M2	0.089 ± 0.017	FS	
OB151771_M1	0.082 ± 0.015	FS	
KB160372-OB161195-MB160350_M1	0.097 ± 0.004	HR	Vandorou et al. (2025b)
KB160372-OB161195-MB160350_M2	0.096 ± 0.003	HR	
MB12323-OB120724_M1	0.084 ± 0.015	FS	Hirao et al. (2016)
OB060109	0.081 ± 0.003	FS-PX	Bennett et al. (2010)
KB161820	0.080 ± 0.009	FS-PX	Jung et al. (2018)
MB140175-OB140676	0.079 ± 0.075	PX	Rattenbury et al. (2017)
KB162142	0.074 ± 0.009	FS-PX	Jung et al. (2018)
MB140547-OB141760	0.069 ± 0.012	FS	Bhattacharya et al. (2016)
MB130618-OB131721	0.064 ± 0.016	FS	Mróz et al. (2017a)
KB170016-OB171392-OB171434-MB170425	0.061 ± 0.004	PX	Udalski et al. (2018)
MB11293	0.059 ± 0.009	HR	Yee et al. (2012)
KB150186-OB151670-OB151673-MB150379	0.058 ± 0.015	FS	Ranc et al. (2019)

spective papers. In particular, accurate models have been proposed taking into account follow-up data, re-reduced photometry and information from CMDs, which allow to exploit the measure of the finite-source effect and fix the angular Einstein angle. In some cases, with a good measure of both the finite-source effect and the microlensing parallax, it has been possible to derive the relative heliocentric proper motion between lens and source. Then, it has been sufficient to multiply by the time baseline to obtain predic-

tions for the expected separation between lens and source. These values are reported in Table 3. When one of these effects is not measured, some Bayesian analysis is eventually needed to infer the properties of the microlensing event, including the proper motion. We have consequently flagged these events in our table. When more than one model fits the data, we have reported the corresponding expectations.

All the expected separations reported in this table are in good agreement with the predictions made by our general

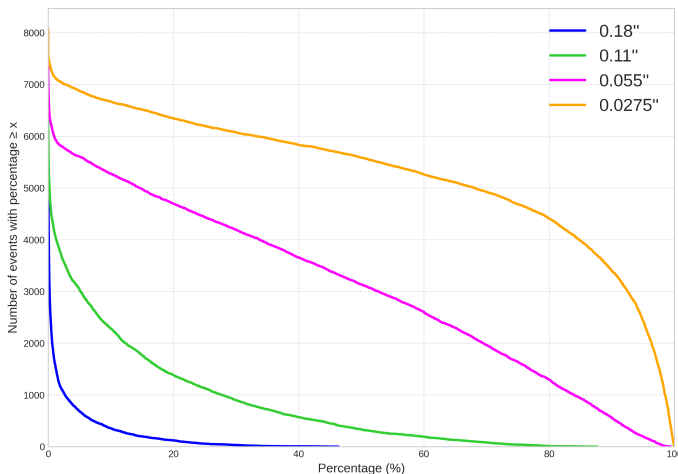


Fig. 11. Number of events with detection probability higher than the given value in the abscissa. Each curve is drawn for a given reference detection threshold.

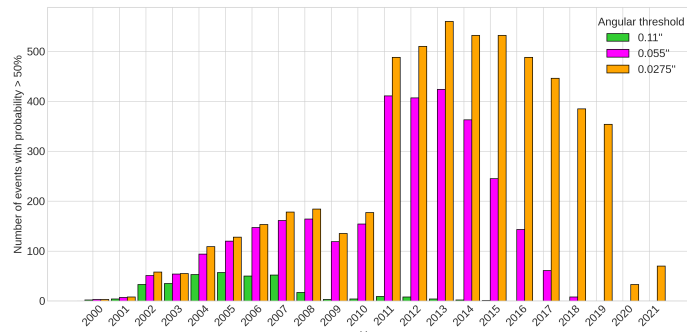


Fig. 12. Number of events with detection probability higher than 50% by year. The three colors refer to three different thresholds reported in the legend.

re-modeling of the original survey data, which makes us more confident with respect to our modeling. Consistently with our full sample of microlensing events, there are just 2 planetary events for which the lens should be separated by more than $0.11''$, 18 events with a separation higher than $0.055''$ and 30 events with separation higher than $0.0275''$.

The two planetary events for which a separation higher than one pixel is predicted are OGLE-2005-BLG-390 (Beaulieu et al. 2006) and MOA-2013-BLG-260/OGLE-2013-BLG-0341 (Gould et al. 2014). The first is a twenty-year-old event, for which a high separation is quite expected. Unfortunately, the lens star should be a faint M-dwarf, while the source is a giant. A high contrast of about 10 magnitudes in this case makes the detection of the faint lens very challenging. The second event is more recent, but since the lens system is relatively close, a high proper motion is derived in the models. Since the source is relatively faint and the lens is made of a binary system of M-dwarfs, this event seems more promising for a successful detection.

The third event in the list is KMT-2016-BLG-0212 Hwang et al. (2018a), which has four possible models in which the lens has mass between 0.36 and $0.45 M_{\odot}$ and the companion could be a brown dwarf or a sub-Neptune depending on the chosen alternative. The different models predict different proper motions and different magnitudes

for source and lens. Therefore, a resolution by *Euclid* should be able to distinguish these alternatives.

6. Conclusions

Decades of microlensing observations towards the bulge have accumulated tens of thousand microlensing events. Thanks to the *Euclid* Galactic Bulge Survey, we have the opportunity to resolve the lens from the source for a substantial fraction of all past microlensing events, bringing the contribution to the knowledge of the Galaxy from microlensing to a higher level.

In this investigation we have compiled the full list of historic events in the footprint of the EGBS. By re-modeling all events in a homogeneous way, we have revised the estimates for the basic microlensing parameters and we have issued predictions for the expected separation of lens and source for more than 8000 microlensing events. In our catalog, astronomers can find all events with their coordinates, baseline magnitude, Einstein time and parallax (if measurable), along with an assessment of the possible category (single lens, binary lens or binary source). The reported chi square in the fit is also useful to discard events based on possible problems with systematics or poor modeling. For each event, we report the probability that the lens is separated from the source by more than one pixel, half pixel, a quarter pixel, or the size of the average PSF. It is clear that the individual cases may feature peculiarities that are not represented in our table and that may pose additional difficulties, such as high contrast between lens and source, a dark lens, additional blended stars, nearby saturated stars. All these can be evaluated and understood only when the real data are available. However, our list represents the starting point and the reference for driving all future detailed analyses of individual microlensing events toward the most promising cases.

We note there is currently an ongoing large *HST* survey of the Roman GBTDS fields (GO-17776; Terry et al. (2024a)). Much like the EGBS, a primary goal of this *HST* precursor survey is to extend the time baseline for which *Roman* lenses and sources can be studied with high-resolution imaging. Joint analysis of the EGBS and *HST* precursor data will allow for robust multi-passband characterization of the lenses in this historical event sample. Further details of the *HST* program will be presented by Terry et al. (in prep).

Finally, the *Roman* Galactic Time Domain Survey (ROTAC 2025) will be extremely useful to prolong the follow-up of historic events and confirm the conclusions of the analyses based on EGBS alone. At the present time, therefore, we are right in the middle of the path to the construction of a broad database of lens-source pairs that can be envisaged as an alternative way to obtain a 3D tomography along our line of sight to the Galactic bulge.

Acknowledgements. The OGLE project has received funding from the Polish National Science Centre grant OPUS-28 2024/55/B/ST9/00447 to AU. The MOA project is supported by JSPS KAKENHI Grant Number JP16H06287, JP22H00153, JP23KK0060 and JP25H00668. This research has made use of publicly available data (<https://kmtnet.kasi.re.kr/ulens/>) from the KMTNet system operated by the Korea Astronomy and Space Science Institute (KASI) at three host sites of CTIO in Chile, SAAO in South Africa, and SSO in Australia. Data transfer from the host site to KASI was supported by the Korea Research Environment Open NETwork (KREONET). VB acknowledges financial support

from PRIN2022 CUP D53D23002590006. This work was supported by the University of Tasmania through the endowed Warren Chair in Astronomy. AAC, J-PB, and ET NR have been supported by the Australian Government through the Australian Research Council Discovery Project Grants 200101909 and 240101842. Research in France has been supported through the SPACE-MLENS ANR grant ANR-24-CE31-3263.

References

Afonso, C., Albert, J. N., Alard, C., et al. 2003, *A&A*, 404, 145
 Alcock, C., Akerlof, C. W., Allsman, R. A., et al. 1993, *Nature*, 365, 621
 Alcock, C., Allsman, R. A., Alves, D. R., et al. 2000a, *ApJ*, 542, 281
 Alcock, C., Allsman, R. A., Alves, D. R., et al. 2000b, *ApJ*, 541, 734
 Bachelet, E. & Penny, M. 2019, *ApJ*, 880, L32
 Bachelet, E., Specht, D., Penny, M., et al. 2022, *A&A*, 664, A136
 Batista, V., Beaulieu, J. P., Gould, A., et al. 2014, *ApJ*, 780, 54
 Beaulieu, J.-P. 2018, *Universe*, 4, 61
 Beaulieu, J. P., Bennett, D. P., Fouqué, P., et al. 2006, *Nature*, 439, 437
 Bennett, D. P., Anderson, J., Bond, I. A., Udalski, A., & Gould, A. 2006, *ApJ*, 647, L171
 Bennett, D. P., Bhattacharya, A., Anderson, J., et al. 2015, *ApJ*, 808, 169
 Bennett, D. P., Bhattacharya, A., Beaulieu, J.-P., et al. 2020, *AJ*, 159, 68
 Bennett, D. P., Bhattacharya, A., Beaulieu, J.-P., et al. 2024, *AJ*, 168, 15
 Bennett, D. P., Rhie, S. H., Nikolaeve, S., et al. 2010, *ApJ*, 713, 837
 Bennett, D. P., Rhie, S. H., Udalski, A., et al. 2016, *AJ*, 152, 125
 Bhattacharya, A., Akeson, R., Anderson, J., et al. 2019, *BAAS*, 51, 520
 Bhattacharya, A., Beaulieu, J. P., Bennett, D. P., et al. 2018, *AJ*, 156, 289
 Bhattacharya, A., Bennett, D. P., Beaulieu, J. P., et al. 2023, *AJ*, 165, 206
 Bhattacharya, A., Bennett, D. P., Bond, I. A., et al. 2016, *AJ*, 152, 140
 Blackman, J. W., Beaulieu, J. P., Cole, A. A., et al. 2021, *AJ*, 161, 279
 Bond, I. A., Abe, F., Dodd, R. J., et al. 2001, *MNRAS*, 327, 868
 Bond, I. A., Bennett, D. P., Sumi, T., et al. 2017, *MNRAS*, 469, 2434
 Bond, I. A., Udalski, A., Jaroszyński, M., et al. 2004, *ApJ*, 606, L155
 Bozza, V. 2024, *A&A*, 688, A83
 Bozza, V., Saggese, V., Covone, G., Rota, P., & Zhang, J. 2025, *A&A*, 694, A219
 Clarke, J. P., Wegg, C., Gerhard, O., et al. 2019, *MNRAS*, 489, 3519
 Cropper, M., Pottinger, S., Niemi, S., et al. 2016, in Society of Photo-Optical Instrumentation Engineers (SPIE) Conference Series, Vol. 9904, Space Telescopes and Instrumentation 2016: Optical, Infrared, and Millimeter Wave, ed. H. A. MacEwen, G. G. Fazio, M. Lystrup, N. Batalha, N. Siegler, & E. C. Tong, 99040Q
 Dominik, M. 2006, *MNRAS*, 367, 669
 Gaia Collaboration, Katz, D., Antoja, T., et al. 2018, *A&A*, 616, A11
 Gaudi, B. S. 2012, *ARA&A*, 50, 411
 Gaudi, B. S., Bennett, D. P., Udalski, A., et al. 2008, *Science*, 319, 927
 Gould, A. 1992, *ApJ*, 392, 442
 Gould, A., Udalski, A., Shin, I. G., et al. 2014, *Science*, 345, 46
 Han, C., Bennett, D. P., Udalski, A., et al. 2019, *AJ*, 158, 114
 Han, C. & Gould, A. 2003, *ApJ*, 592, 172
 Hirao, Y., Bennett, D. P., Ryu, Y.-H., et al. 2020, *AJ*, 160, 74
 Hirao, Y., Udalski, A., Sumi, T., et al. 2016, *ApJ*, 824, 139
 Hwang, K. H., Kim, H. W., Kim, D. J., et al. 2018a, *Journal of Korean Astronomical Society*, 51, 197
 Hwang, K. H., Udalski, A., Shvartzvald, Y., et al. 2018b, *AJ*, 155, 20
 Jung, Y. K., Gould, A., Udalski, A., et al. 2019, *AJ*, 158, 28
 Jung, Y. K., Hwang, K.-H., Ryu, Y.-H., et al. 2018, *AJ*, 156, 208
 Kim, H.-W., Hwang, K.-H., Gould, A., et al. 2021, *AJ*, 162, 15
 Kim, S.-L., Lee, C.-U., Park, B.-G., et al. 2016, *Journal of Korean Astronomical Society*, 49, 37
 Koshimoto, N., Baba, J., & Bennett, D. P. 2021, *ApJ*, 917, 78
 Koshimoto, N. & Ranc, C. 2022, nkoshimoto/genulens: Release version 1.2
 Kunder, A., Koch, A., Rich, R. M., et al. 2012, *AJ*, 143, 57
 Lam, C. Y., Lu, J. R., Udalski, A., et al. 2022, *ApJ*, 933, L23
 Mao, S. & Paczynski, B. 1991, *ApJ*, 374, L37
 Mellier, Y., Abdurro'uf, Acevedo Barroso, J. A., et al. 2025, *A&A*, 697, A1
 Mróz, P., Udalski, A., Bond, I. A., et al. 2017a, *AJ*, 154, 205
 Mróz, P., Udalski, A., Skowron, J., et al. 2017b, *Nature*, 548, 183
 Mróz, P., Udalski, A., Skowron, J., et al. 2019, *ApJS*, 244, 29
 Mróz, P., Udalski, A., Szymański, M. K., et al. 2024a, *ApJ*, 976, L19
 Mróz, P., Udalski, A., Szymański, M. K., et al. 2024b, *Nature*, 632, 749
 Nataf, D. M., Gould, A., Fouqué, P., et al. 2013, *ApJ*, 769, 88
 Niikura, H., Takada, M., Yasuda, N., et al. 2019, *Nature Astronomy*, 3, 524
 Nunota, K., Sumi, T., Koshimoto, N., et al. 2025, *ApJ*, 979, 123
 Paczynski, B. 1986, *ApJ*, 304, 1
 Penny, M. T., Kerins, E., Rattenbury, N., et al. 2013, *MNRAS*, 434, 2
 Racca, G. D., Laureijs, R., Stagnaro, L., et al. 2016, in Society of Photo-Optical Instrumentation Engineers (SPIE) Conference Series, Vol. 9904, Space Telescopes and Instrumentation 2016: Optical, Infrared, and Millimeter Wave, ed. H. A. MacEwen, G. G. Fazio, M. Lystrup, N. Batalha, N. Siegler, & E. C. Tong, 99040O
 Ranc, C., Bennett, D. P., Hirao, Y., et al. 2019, *AJ*, 157, 232
 Rattenbury, N. J., Bennett, D. P., Sumi, T., et al. 2017, *MNRAS*, 466, 2710
 Refsdal, S. 1966, *MNRAS*, 134, 315
 Robin, A. C., Reylé, C., Derrière, S., & Picaud, S. 2003, *A&A*, 409, 523
 ROTAC. 2025, arXiv e-prints, arXiv:2505.10574
 Sahu, K. C., Anderson, J., Casertano, S., et al. 2022, *ApJ*, 933, 83
 Schlaufly, E. F. & Finkbeiner, D. P. 2011, *ApJ*, 737, 103
 Schlegel, D. J., Finkbeiner, D. P., & Davis, M. 1998, *ApJ*, 500, 525
 Shvartzvald, Y., Yee, J. C., Calchi Novati, S., et al. 2017, *ApJ*, 840, L3
 Street, R. A., Udalski, A., Calchi Novati, S., et al. 2016, *ApJ*, 819, 93
 Sumi, T., Abe, F., Bond, I. A., et al. 2003, *ApJ*, 591, 204
 Sumi, T., Bennett, D. P., Bond, I. A., et al. 2013, *ApJ*, 778, 150
 Sumi, T., Koshimoto, N., Bennett, D. P., et al. 2023, *AJ*, 166, 108
 Terry, S., Abrams, N., Anderson, J., et al. 2024a, A Precursor Survey of the Roman Galactic Bulge Time Domain Fields, HST Proposal. Cycle 32, ID. #17776
 Terry, S. K., Bachelet, E., Zohrabi, F., et al. 2025, arXiv e-prints, arXiv:2510.13974
 Terry, S. K., Beaulieu, J.-P., Bennett, D. P., et al. 2024b, *AJ*, 168, 72
 Tisserand, P., Le Guillou, L., Afonso, C., et al. 2007, *A&A*, 469, 387
 Tsapras, Y. 2018, *Geosciences*, 8, 365
 Udalski, A., Ryu, Y. H., Sajadian, S., et al. 2018, *Acta Astron.*, 68, 1
 Udalski, A., Szymanski, M., Kaluzny, J., et al. 1993, *Acta Astron.*, 43, 289
 Udalski, A., Szymanski, M., Kaluzny, J., Kubiak, M., & Mateo, M. 1992, *Acta Astron.*, 42, 253
 Udalski, A., Szymanski, M., Kaluzny, J., et al. 1994a, *Acta Astron.*, 44, 227
 Udalski, A., Szymanski, M., Stanek, K. Z., et al. 1994b, *Acta Astron.*, 44, 165
 Udalski, A., Szymanski, M. K., & Szymanski, G. 2015, *Acta Astron.*, 65, 1
 Vandorou, A., Bennett, D. P., Beaulieu, J.-P., et al. 2020, *AJ*, 160, 121
 Vandorou, A., Bennett, D. P., Beaulieu, J.-P., et al. 2025a, arXiv e-prints, arXiv:2504.06347
 Vandorou, A., Dang, L., Bennett, D. P., et al. 2025b, *AJ*, 169, 319
 Witt, H. J. & Mao, S. 1994, *ApJ*, 430, 505
 Wyrzykowski, L., Skowron, J., Kozłowski, S., et al. 2011, *MNRAS*, 416, 2949
 Yang, H., Mao, S., Zang, W., & Zhang, X. 2021, *MNRAS*, 502, 5631
 Yee, J. C., Shvartzvald, Y., Gal-Yam, A., et al. 2012, *ApJ*, 755, 102
 Zhang, X., Zang, W., Udalski, A., et al. 2020, *AJ*, 159, 116

¹ Dipartimento di Fisica "E.R. Caianiello", Università di Salerno, Via Giovanni Paolo 132, Fisciano, I-84084, Italy

² Istituto Nazionale di Fisica Nucleare, Sezione di Napoli, Via Cintia, Napoli, I-80126, Italy

³ Université Marie et Louis Pasteur, CNRS, Institut UTINAM UMR 6213, Besançon, France

⁴ Greenhill Observatory & School of Natural Sciences, University of Tasmania, P.O. Box 807, Sandy Bay, TAS 7006 Australia

- ⁵ Sorbonne Université, CNRS UMR 7095, Institut d’Astrophysique de Paris, 98 bis bd Arago, 75014 Paris, France
- ⁶ Université Paris-Saclay, Université Paris Cité, CEA, CNRS, AIM, 91191, Gif-sur-Yvette, France
- ⁷ Jodrell Bank Centre for Astrophysics, University of Manchester, Oxford Road, Manchester, M13 9PL, UK
- ⁸ Astronomical Observatory, University of Warsaw, Al. Ujazdowskie 4, 00-478 Warszawa, Poland
- ⁹ Department of Physics and Astronomy, Louisiana State University, Baton Rouge, LA 70803 USA
- ¹⁰ Department of Physics, University of Warwick, Gibbet Hill Road, Coventry, CV4 7AL, UK
- ¹¹ Villanova University, Department of Astrophysics and Planetary Sciences, 800 Lancaster Ave., Villanova, PA 19085, USA
- ¹² Institute for Space-Earth Environmental Research, Nagoya University, Nagoya 464-8601, Japan
- ¹³ Code 667, NASA Goddard Space Flight Center, Greenbelt, MD 20771, USA
- ¹⁴ Department of Astronomy, University of Maryland, College Park, MD 20742, USA
- ¹⁵ School of Mathematical and Computational Sciences, Massey University, Auckland 0745, New Zealand
- ¹⁶ Department of Earth and Space Science, Graduate School of Science, Osaka University, Toyonaka, Osaka 560-0043, Japan
- ¹⁷ Institute of Astronomy, Graduate School of Science, The University of Tokyo, 2-21-1 Osawa, Mitaka, Tokyo 181-0015, Japan
- ¹⁸ Institute of Space and Astronautical Science, Japan Aerospace Exploration Agency, 3-1-1 Yoshinodai, Chuo, Sagamihara, Kanagawa 252-5210, Japan
- ¹⁹ Department of Physics, University of Auckland, Private Bag 92019, Auckland, New Zealand
- ²⁰ University of Canterbury Mt. John Observatory, P.O. Box 56, Lake Tekapo 8770, New Zealand